# Dirac scatteredwave calculations for Ag2+ 3, Au q+ 3, and Au q+ 4 (q=1, 2) clusters

Ramiro ArratiaPerez and Gulzari L. Malli

Citation: The Journal of Chemical Physics **84**, 5891 (1986); doi: 10.1063/1.449900
View online: http://dx.doi.org/10.1063/1.449900
View Table of Contents: http://scitation.aip.org/content/aip/journal/jcp/84/10?ver=pdfcov
Published by the AIP Publishing



# Dirac scattered-wave calculations for $Ag_3^{2+}$, $Au_3^{q+}$, and $Au_4^{q+}$ ($q = 1, 2$) clusters[a)]

Ramiro Arratia-Perez and Gulzari L. Malli
*Department of Chemistry and Theoretical Science Institute, Simon Fraser University, Burnaby, British Columbia, Canada V5A 1S6*

(Received 23 October 1985; accepted 22 January 1986)

Dirac scattered-wave (DSW) calculations are presented for the $Ag_3^{2+}$, $Au_3^{+}$, $Au_3^{2+}$, $Au_4^{+}$, and $Au_4^{2+}$ clusters. The results show that relativistic effects in bonding are not negligible for the silver cluster; whereas for the gold clusters these are very significant and lead to appreciable *s–d* hybridization in the bonding molecular orbitals. Zeeman and hyperfine tensors have been calculated for the $Ag_3^{2+}$, which are in very good agreement with the experimental results. These tensors are also predicted for the $Au_3^{2+}$ cluster. First ionization potentials and excitation energies are predicted for all these cationic clusters using the spin-restricted transition state method. Contour diagrams which clearly reveal the significant relativistic effects in bonding are also presented.

## I. INTRODUCTION

During the last decade, there has been considerable interest in the bare metal clusters[1,2] because of their relevance to surface phenomena and heterogeneous catalysis.[3,4] Recent gas phase spectroscopic studies[5] have suggested a distorted Jahn–Teller $D_{3h}$ geometry for the copper trimer ($Cu_3$), in both the ground and the excited states. The ESR spectra of the silver trimer ($Ag_3$) in inert matrices[6] indicate a $C_{2v}$ geometry which arises from a Jahn–Teller distortion of the $D_{3h}$ geometry (in $^2E'$ state). Theoretical studies using the relativistic effective core potential,[7] as well as the local-density nonrelativistic pseud otential[8] methods, also predict the $C_{2v}$ geometry for $Ag_3$. However, both the above-mentioned theoretical methods[7,8] predict the $D_{3h}$ geometry for both the $Cu_3^+$ and $Ag_3^+$ clusters. Furthermore, the ESR spectra of the cationic silver clusters in frozen aqueous glasses of silver salts[9,10] favor a triangular ($D_{3h}$) geometry for $Ag_3^{2+}$ and a tetrahedral ($T_d$) geometry for $Ag_4^{3+}$.

Although a large number of low nuclearity bare cationic gold clusters have been generated by a variety of techniques,[11–13] no experimental data are available at present about their electronic structure, optical spectra, and magnetic properties. Moreover, it is now well established that relativity significantly modifies the behavior of not only the core but also the valence electrons in a heavy element.[14,15] It has been further recognized[16] for a heavy element that the relativistic effects are too large to be accurately treated by the first order perturbation method of taking the expectation value of operators, such as the spin-orbit coupling which describe relativistic corrections.

In order to investigate the importance of relativistic effects on chemical bonding, optical spectra, and ionization potentials of heavy element clusters, we report here fully relativistic self-consistent-field (SCF) Dirac scattered-wave (DSW) calculations for $Ag_3^{2+}$, $Au_3^{q+}$, and $Au_4^{q+}$ ($q = 1,2$) clusters. In addition, Zeeman and hyperfine tensors are calculated for the paramagnetic $Ag_3^{2+}$ and $Au_3^{2+}$ clusters using the SCF-DSW four-component wave functions.

## II. DIRAC SCATTERED-WAVE (DSW) CALCULATIONS

The Dirac scattered-wave (DSW) method is the relativistic version of the nonrelativistic (NR) scattered-wave (SW) self-consistent-field method. The DSW method has been thoroughly reviewed[17–19] and the reader is referred to these reviews for further details. This method has expanded the scope of relativistic electronic structure calculations on systems containing heavy atoms.[20–25] In particular, the method has been found very useful for understanding the relativistic effects in electronic structure, optical spectra, and magnetic properties for systems which are too large or too heavy for reliable high quality *ab initio* fully relativistic calculations at present.

The DSW method employs the same exchange and potential approximations as in its nonrelativistic counterpart, but uses the Dirac equation rather than the Schrödinger equation to generate the one-electron orbitals. Thus, relativistic effects such as spin-orbit interaction, Darwin, and mass-velocity corrections are included at the SCF stage.

The Dirac equation[26] for a single electron in an external molecular potential $V$ reads as follows:

$$\{c\alpha \cdot p + \beta mc^2 + V\}\Psi_i = \epsilon_i \Psi_i, \tag{1}$$

where in Eq. (1) the one-electron wave function $\Psi_i$ is a four-component spinor, $p$ is the linear momentum operator, and $\alpha$ and $\beta$ are the standard Dirac matrices. The potential $V$ is the sum of the Coulomb potentials arising from the nuclei and electrons and an exchange-correlation term, for which Slater's local density approximation[27] is used. For each orbital, the wave function inside the atomic spheres is written as a linear combination of the spinors $|\kappa, \mu\rangle$, where

$$|\kappa, \mu\rangle = \begin{pmatrix} g(r)\chi_{\kappa\mu}(\theta,\phi) \\ if(r)\chi_{-\kappa\mu}(\theta,\phi) \end{pmatrix}. \tag{2}$$

In Eq. (2) the $g(r)$ and $f(r)$ are the radial functions, determined by numerical integration of the radial Dirac equations

[a)] Presented as an invited poster at the 5th International Congress on Quantum Chemistry (ICQC), Montreal, August 1985.

 0021-9606/86/105891-07$02.10  

and $\chi_{\kappa\mu}(\theta,\phi)$ are the two-component spherical spinors.[26] The molecular spinors ($\Psi_i$) are taken to transform according to the extra (or additional) irreducible representations of the molecular double point group of the system under investigation, and the one-electron orbital energies ($\epsilon_i$) are determined by solving the DSW secular equations.

We assumed the $D_{3h}$ and the $T_d$ geometries for the trimeric and the tetrameric cationic clusters, since the ESR studies[9,10] favor these geometries for the $Ag_3^{2+}$ ($D_{3h}$) and $Ag_4^{3+}$ ($T_d$) clusters, respectively. The size of the sphere radii were chosen according to the procedure suggested by Norman[28] and these "atomic number radii" were scaled by a factor of 0.88, which has been found optimal in many DSW calculations on heavy element systems.[21-24] A minimum basis of angular functions was used, with $l \leqslant 4$ on the outer sphere and $l \leqslant 2$ on the metal. The parameters and the geometries used for the various cationic clusters are given in Table I. The nonrelativistic calculations were obtained by using a large value of $c = 10^{15}$ a.u. in order to estimate quantitatively the relativistic effects.

## III. RESULTS AND DISCUSSION

### A. $Ag_3^{2+}$

The nonrelativistic (NR) and the relativistic (DSW) valence molecular orbital energy diagrams for $Ag_3^{2+}$ are shown in Fig. 1. The nonrelativistic results show a filled $\tilde{d}$ band which consists of bonding, nonbonding, and antibonding MO's arising from appropriate combinations of the 4*d* atomic orbitals. The highest occupied molecular orbital (HOMO), $3a_1'$, is a bonding MO which is singly occupied, and it is a hybrid of 5*s*–5*p* atomic orbitals (75% 5*s*, 15% 5*p*, and 6% 4*d*). The lowest unoccupied molecular orbital (LUMO), 4*e'*, is, however, an antibonding MO and it is also a hybrid of 5*s*–5*p* (77% 5*s*, 18% 5*p*, and 5% 4*d*) atomic orbitals.

It is interesting to note that apart from the bonding $3a_1'$ MO, the lower lying occupied molecular orbitals ($1a_1'$ and $1e'$) which are combinations of almost pure 4*d* metal orbitals, also participate in the cluster bonding. This can be seen from the nonrelativistic wave function contour plot of one of these molecular orbitals ($1a_1'$) shown in Fig. 2. The participation of the 4*d* orbitals in bonding in $Ag_3^{2+}$ is rather unexpected, because in a previous NR-SW[30] and an *ab initio* NR-SCF[31] calculation on $Ag_2$, the 4*d* orbitals were found to behave as core-like with no participation in bonding.

Since it is well known that relativistic effects stabilize the *s* and *p* orbitals but destabilize *d* orbitals in the Ag atom,[15] the unoccupied ($6e_2$,$6e_3$) and the HOMO ($6e_1$) levels are stabilized in the $Ag_3^{2+}$ cluster, while the occupied molecular orbitals lying below the HOMO are destabilized. Furthermore, spin-orbit interaction splits the 4*e'* (NR-LUMO) level into the $6e_2$ and $6e_3$ MO's by $\sim 286\ cm^{-1}$ and the occupied $\tilde{d}$ band into the $\tilde{d}_{3/2}$ and the $\tilde{d}_{5/2}$ subbands by $\sim 0.82$ eV. The calculated splitting of the $\tilde{d}$ band for $Ag_3^{2+}$ is in good agreement with the value of $\sim 0.84$ eV for this splitting from the photoemission experiments on a low coverage of silver on a carbon substrate,[32] and with the calculated value of 1.07 eV for this splitting in $Ag_2$.[33]

Further analysis of the results for $Ag_3^{2+}$ shows that the relativistic effects increase the *d* bandwidth by $\sim 0.3$ eV (see Fig. 1) and stabilize the HOMO (as well as the LUMO) by $\sim 0.7$ eV. This demonstrates that, as expected, the relativistic effects in $Ag_3^{2+}$ are not very large, as can also be deduced from the total valence populations given in Table II. Among the *d* orbitals the $d_{3/2}$ and $d_{5/2}$ orbitals are equally populated, and the population ratio is 1.50 which is equal to the nonrelativistic limit. However, among the *p* orbital the lower energy $p_{1/2}$ spinors are favored over the $p_{3/2}$ spinor; the $p_{3/2}$:$p_{1/2}$ population ratio is 1.70 in the DSW calculation but a value of

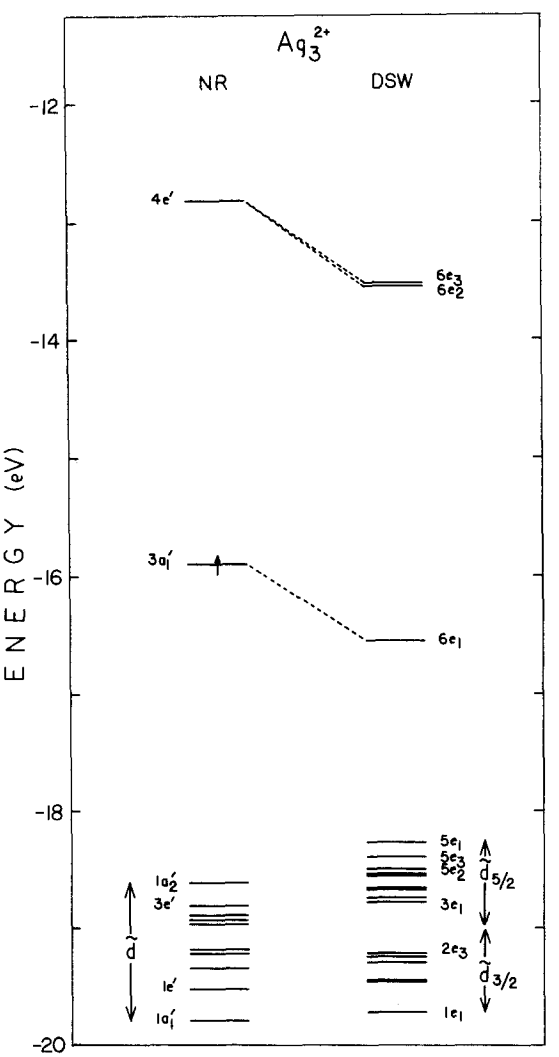


FIG. 1. Nonrelativistic (NR) and relativistic (DSW) valence energy levels of $Ag_3^{2+}$.

TABLE I. Parameters used in the calculations.[a]

| | $Ag_3^{2+}$ | $Au_3^{q+}$ | $Au_4^{q+}$ |
|---|---|---|---|
| M–M distance (Å) | 2.88 | 2.70 | 2.70 |
| Point group symmetry | $D_{3h}$ | $D_{3h}$ | $T_d$ |
| $\alpha_M = \alpha_{IS} = \alpha_{OUT}$ | 0.70145 | 0.69301 | 0.69301 |
| $b_{OUT}$ | 3.24 | 3.03 | 3.06 |
| $b_M$ | 1.66 | 1.58 | 1.51 |

[a] *b* denotes sphere radius (in Å) and $\alpha$ is the exchange parameter (from Ref. 29). IS stands for the intersphere region, and $q = 1,2$.

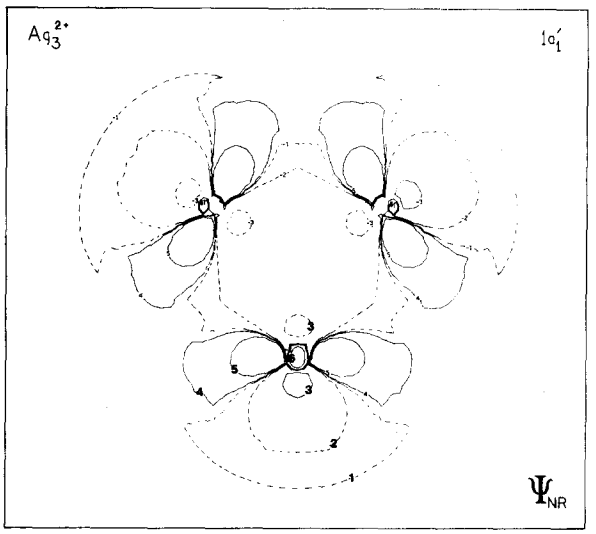


FIG. 2. Contours of the nonrelativistic $1a_1'$ MO of $Ag_3^{2+}$. Contour values (electron/bohr$^3$)$^{1/2}$ are: (1,8), (2,7), (3,6), (4,5) = $\pm 0.2$, $\pm 0.02$, $\pm 0.002$, and $\pm 0.0002$. These values are the same for all the contours presented here. Negative contours are represented by dashed lines.

2.00 is required by symmetry in the nonrelativistic limit. Moreover, the relativistic stabilization of the HOMO ($6e_1$) of $Ag_3^{2+}$, which is a bonding molecular orbital (shown in Fig. 3), agrees with the observation that the relativistic effects contract the bond length of $Ag_2$ by $\sim 0.2$ a.u.[34] Furthermore, apart from the HOMO ($6e_1$), there are in addition bonding orbitals ($1e_2$, $1e_1$, $1e_3$, and $2e_2$) which are primarily $4d_{3/2}$-like, and there are antibonding ($5e_1$, $5e_2$, and $5e_3$) MO's which are $4d_{5/2}$-like orbitals located in $\tilde{d}_{5/2}$.

From the above analysis, it is clear that the relativistic effects in bonding for $Ag_3^{2+}$ are unimportant but nonnegligible, since there is no significant $s$–$d$ hybridization in the bonding molecular orbitals. This is in contrast to the bonding characteristics found for the cationic gold clusters, as discussed in Sec. III B.

### B. $Au_3^+$, $Au_3^{2+}$, $Au_4^+$, and $Au_4^{2+}$

The nonrelativistic (NR) as well as the relativistic (DSW) valence energy levels were calculated for $Au_3^{q+}$ and $Au_4^{q+}$ ($q = 1,2$) clusters. In Fig. 4 we present these results only for $Au_3^+$ and $Au_4^+$ as representatives of the trimeric ($D_{3h}$) and the tetrameric ($T_d$) clusters, respectively. Our nonrelativistic (NR) calculations indicate that the bonding HOMO's ($3a_1'$) in $Au_3^{q+}$ are essentially 6$s$–6$p$ hybrids (80% 6$s$, 13% 6$p$, and 7% 5$d$) and, in addition there are small contributions to the bonding from the $1a_1'$, $1e'$, and $1a_2''$ molecular orbitals which are mostly combinations of 5$d$-like atomic orbitals. In $Au_4^+$, the HOMO $4t_2$, however, is an antibonding MO which is a hybrid of 6$s$–6$p$ orbitals (57% 6$s$, 36% 6$p$, and 7% 5$d$). In the case of $Au_4^{2+}$ the HOMO $2a_1$ is a bonding MO (as in $Au_4^+$) and again it consists of a hybrid of 6$s$–6$p$ orbitals (78% 6$s$, 14% 6$p$, and 8% 5$d$). Thus, in both the tetrahedral cationic gold clusters, the bonding is dominated by the 6$s$–6$p$ hybrid orbitals $2a_1$ with minor contributions to the bonding from the $1a_1$, $1t_1$, and $1t_2$ molecular orbitals which are almost pure 5$d$-like atomic orbitals. Furthermore, there are antibonding MO's ($2t_1$ and $3t_2$) which consist of combinations of almost pure $d$-like orbitals.

The relativistic valence molecular orbital energy levels for $Au_3^{q+}$ and $Au_4^{q+}$ ($q = 1,2$) are shown in Fig. 5. The most notable characteristic of the valence structure in each cluster is the large splitting of the occupied $\tilde{d}$ band into the $\tilde{d}_{3/2}$ and $\tilde{d}_{5/2}$ bands due to the spin-orbit interaction and this splitting is $\sim 2.00$ and $\sim 2.35$ eV in $Au_3^{q+}$ and $Au_4^{q+}$, respectively, which agrees with the value of 2.04 eV calculated for this splitting in $Au_2$.[33] The total valence populations for the various cationic clusters are collected in Table II. It can be seen that the $d_{5/2}$:$d_{3/2}$ population ratios are very close to the NR limit of 1.50, while the $p_{3/2}$:$p_{1/2}$ population ratios are very different from the NR value of 2.00, indicating that the lower energy $p_{1/2}$ spinors are largely favored over the $p_{3/2}$ atomic spinors. Furthermore, comparison of the total relativistic and the nonrelativistic (not shown) valence populations indicated that the net relativistic effect on the charge distributions leads to a transfer of $\sim 0.4$ and $\sim 1.1$ electrons from 5$d$ to 6$s$ atomic orbitals in $Au_n^+$ and $Au_n^{2+}$ ($n = 3,4$), respectively. These bring about a relativistic stabilization of the molecular orbitals containing 6$s$ atomic orbitals and a relativistic destabilization of the MO's involving 5$d$ atomic orbitals. The relativistic bonding differs considerably from the

TABLE II. Total valence populations of cationic clusters.[a]

| $l$ | $j$ | $Ag_3^{2+}$ | $Au_3^+$ | $Au_3^{2+}$ | $Au_4^+$ | $Au_4^{2+}$ |
|---|---|---|---|---|---|---|
| $s$ | 1/2 | 0.343 | 0.788 | 0.742 | 0.820 | 0.643 |
| | 1/2 | 0.040 | 0.087 | 0.077 | 0.167 | 0.099 |
| $p$ | | 1.70[b] | 1.33 | 1.37 | 0.80 | 1.31 |
| | 3/2 | 0.068 | 0.116 | 0.106 | 0.134 | 0.130 |
| Total $p$ | | 0.108 | 0.203 | 0.183 | 0.301 | 0.229 |
| | 3/2 | 3.946 | 3.879 | 3.856 | 3.884 | 3.870 |
| $d$ | | 1.50 | 1.49 | 1.44 | 1.48 | 1.48 |
| | 5/2 | 5.936 | 5.797 | 5.552 | 5.745 | 5.758 |
| Total $d$ | | 9.882 | 9.676 | 9.408 | 9.629 | 9.628 |
| Total M | | 10.333 | 10.667 | 10.333 | 10.750 | 10.500 |

[a] The charge in the intersphere and outer sphere regions has been partitioned among the atoms according to the algorithm of Ref. 35.

[b] Ratio of populations for the $j = l + 1/2$ to $j = l - 1/2$. In the NR limit these ratios are required to be $(l+1)/l$ (for $l > 0$).

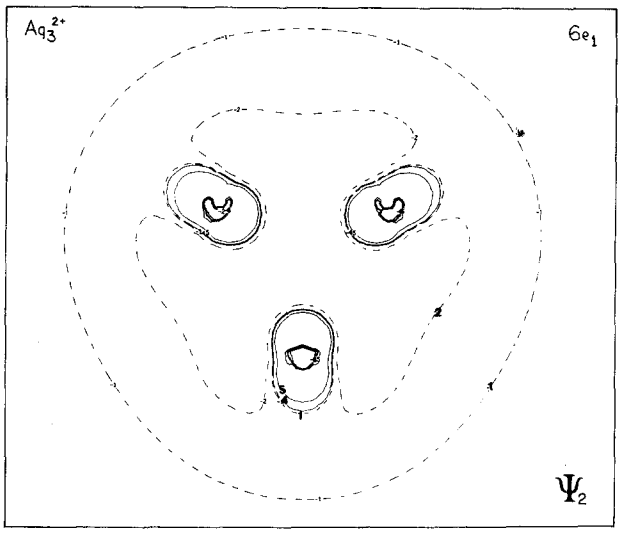


FIG. 3. Contours of the dominant $6e_1$ wave function component of $Ag_3^{2+}$.

nonrelativistic bonding analysis described above. The highest occupied molecular orbitals (HOMO), viz. $6e_1$ of $Au_3^{q+}$ and $7q$ of $Au_4^{2+}$ (see Fig. 5), arise primarily from the metal $5d_{5/2}$ atomic spinors, whereas the HOMO $4e_3$ in $Au_4^+$ is mostly a $6s_{1/2}$–$6p_{1/2}$ hybrid. One would expect $Au_3^{2+}$ and $Au_4^+$ to be paramagnetic, while $Au_3^+$ and $Au_4^{2+}$ to be diamagnetic. The HOMO's ($6e_1$) in $Au_3^{q+}$ are essentially antibonding combinations of the $5d_{5/2}$ spinors, as can be seen in Fig. 6, where we show only the contours of the dominant component of the HOMO ($6e_1$) of $Au_3^+$. It is interesting to contrast the $6e_1$ MO of $Ag_3^{2+}$ (shown in Fig. 3), which is a bonding orbital, against the $6e_1$ MO of $Au_3^+$. Furthermore, in $Ag_3^{2+}$ the characters of the NR-HOMO bonding orbital $3a_1'$ and the relativistic $6e_1$ (Fig. 3) are surprisingly seen in the relativistic molecular orbitals $3e_1$ and $5e_1$ (to a lesser extent), respectively, which are located below the HOMO $6e_1$. This is illustrated in the contour shown in Fig. 7 for the $3e_1$ molecular orbital of $Au_3^+$ (which is the same for $Au_3^{2+}$). Moreover, in contrast to both the silver cationic cluster, and to the nonrelativistic bonding description of gold clusters, the contributions of the $6p$ orbitals to the valence electronic structure are essentially nonbonding. This conclusion is supported by the contour of $\Psi_1$ component of the $3e_1$ relativistic MO. Therefore, the NR description of the dominant role of the $6s$–$6p$ hybrid in bonding is unrealistic in these cationic gold clusters. On the contrary, the orbital decomposition of the $5e_1$ and $3e_1$ bonding molecular spinors of $Au_3^+$ show

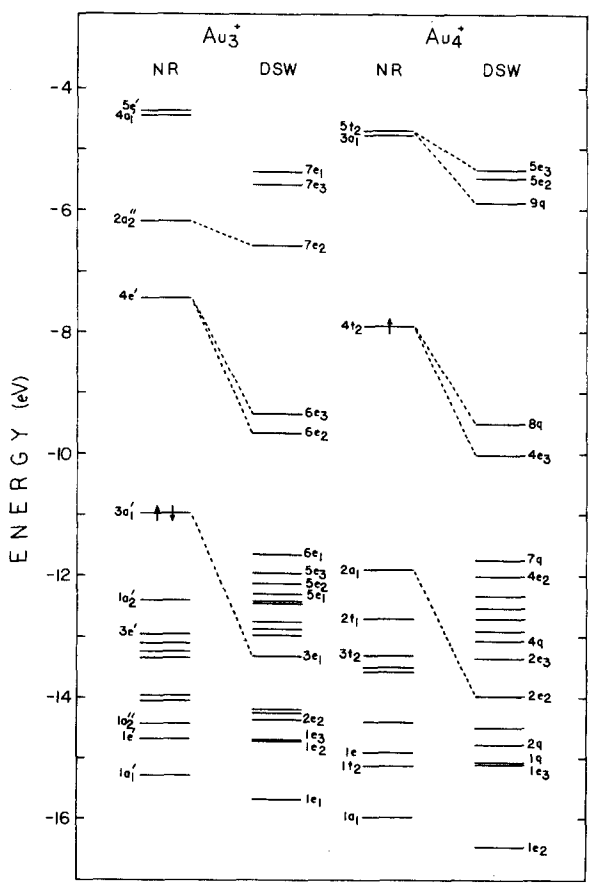


FIG. 4. Nonrelativistic (NR) and relativistic (DSW) valence energy levels of $Au_3^+$ and $Au_4^+$. The HOMOs for $Au_3^+$ are $3a_1'$ (NR) and $6e_1$ (DSW), and for $Au_4^+$ are $4t_2$ (NR) and $4e_3$ (DSW). Note the relativistic stabilization of the bonding MO's $3a_1'$ and $2a_1$, see the text.

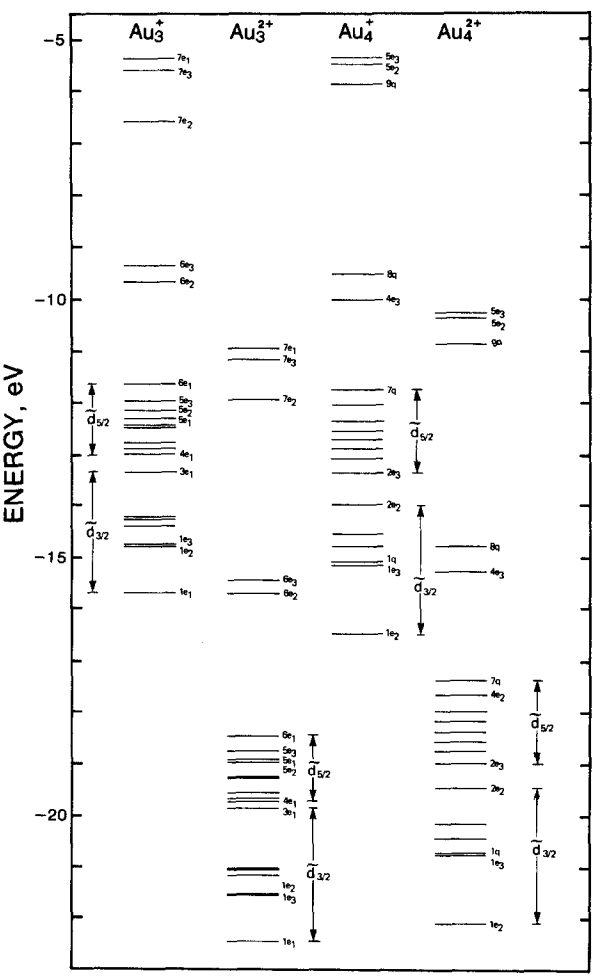


FIG. 5. Relativistic valence energy levels of $Au_3^+$, $Au_3^{2+}$, $Au_4^+$, and $Au_4^{2+}$. The HOMOs are: $6e_1$, $6e_1$, $4e_3$, and $7q$, respectively. Double group notation is used: "$e$" orbitals are twofold degenerate and "$q$" orbitals are fourfold degenerate.

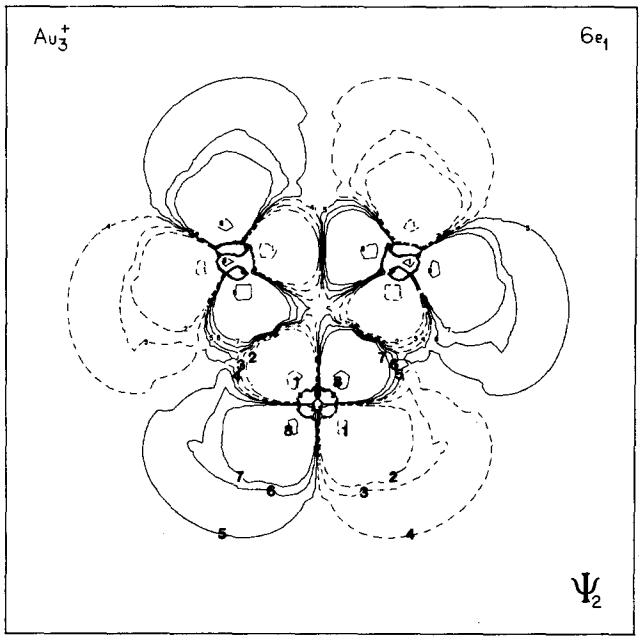


FIG. 6. Contours of the dominant $6e_1$ wave function component of $Au_3^+$.

significant "*s–d*" hybridization; e.g., in $Au_3^{q+}$ the $5e_1$ molecular spinors are mostly $6s_{1/2}$–$5d_{5/2}$ hybrids (16% $6s_{1/2}$–80% $5d_{5/2}$), while the $3e_1$ molecular spinors contain large contributions from the $6s_{1/2}$ and $5d_{3/2}$ waves (46% $6s_{1/2}$–47% $5d_{3/2}$). In $Au_3^{2+}$ we observe a more balanced *s–d* hybridization, e.g., the $5e_1$ MO consist of 33% $6s_{1/2}$ and 65% $d_{5/2}$, while the $3e_1$ MO consists of 31% $6s_{1/2}$ and 48% $5d_{3/2}$. Rabii and Yang[33] arrived at the same conclusion from their study of $Au_2$. The relativistic stabilization of the bonding $3e_1$ molecular orbital is 2.35 and 3.10 eV in $Au_3^+$ and $Au_3^{2+}$, respectively. The corresponding values obtained for $Au_2$ are 2.14 and 1.92 eV, by the DSW[33] and the ECP[36] methods, respectively. About 2 eV higher than the HOMO ($6e_1$) lie the orbitals $6e_2$ and $6e_3$, which arise due to the spin-orbit splitting of the NR $4e'$ orbital. The magnitude of this splitting ($\sim$0.32 eV) in $Au_3^{q+}$ almost equals the $6p_{1/2}$–$6p_{3/2}$ energy separation of 0.47 eV in the Au atom.[37] The analysis of our results for $Au_4^+$ shows that the HOMO ($4e_3$) is an antibonding $6s_{1/2}$–$6p_{1/2}$ hybrid which is stabilized by $\sim$2.10 eV. The corresponding NR ($4t_2$) HOMO splits by spin-orbit interaction into the twofold ($4e_3$) and the fourfold degenerate $8q$ MO's. The magnitude of this splitting is quite large (0.51 eV). The NR calculation places the bonding $2a_1$ (6*s*–6*p* hybrid) below the HOMO $4t_2$, while the DSW calculation places an antibonding fourfold degenerate $7q$ MO below the HOMO $4e_3$, consisting mostly of $5d_{5/2}$ atomic spinors. Furthermore, the bonding molecular orbital ($2e_2$) is stabilized by 2.10 eV and consists of a $6s_{1/2}$–$5d_{3/2}$ hybrid (52% $6s_{1/2}$–40% $5d_{3/2}$). The lowest occupied (valence) molecular spinor ($1e_2$) is also a bonding MO and shows $6s_{1/2}$–$5d_{3/2}$–$5d_{5/2}$ hybridization. In addition, the $1e_3$ and the $1q$ MO's (which consist of 70% $5d_{3/2}$, 25% $5d_{5/2}$, and 5% $6s_{1/2}$) also contribute to the overall cluster bonding. The bonding characteristics of the $Au_4^{q+}$ clusters are very similar and in both the tetrahedral clusters there are $6s_{1/2}$ contributions to the $\tilde{d}_{3/2}$ and $\tilde{d}_{5/2}$ bands.

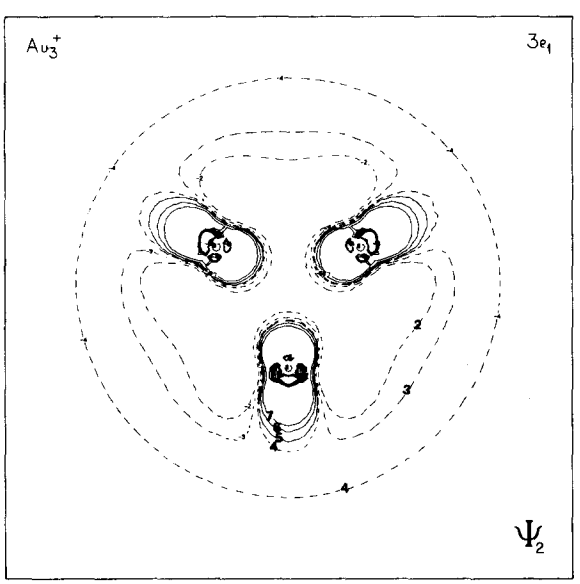


FIG. 7. Contours of the dominant $3e_1$ wave function component of $Au_3^+$.

## IV. ZEEMAN AND HYPERFINE INTERACTIONS

The method used for estimating *g* tensors and molecular hyperfine interactions is based upon a first order perturbation to the Dirac Hamiltonian so that the effects of magnetic fields are described by the perturbation operator $H'$,[21,23] where

$$H' = e\alpha \cdot A. \tag{3}$$

In Eq. (3) $\alpha$ is the vector of Dirac matrices and $A$ is the electromagnetic vector potential. For the Zeeman interaction $A = 1/2\ (B \times r)$, where $B$ is the external magnetic field. For the hyperfine term $A = (\mu \times r)/r^3$ where $\mu$ is the nuclear magnetic moment. Matrix elements of these operators are evaluated in the basis spanning the two rows of the $e_1$ representation of the HOMO of $M_3^{2+}$ (M = Ag,Au). The details of the evaluation of the angular and the radial integrals have been described elsewhere.[21,23] The resulting perturbation energies are then fitted to the usual spin Hamiltonian[23]:

$$H_{\text{spin}} = S \cdot g \cdot B + S \cdot A_{\text{hf}} \cdot I, \tag{4}$$

where in Eq. (4), a value of $S = 1/2$ is used in the spin Hamiltonian, a convenient parametrization to describe the ground state Kramer's doublet,[23] and $I$ is the nuclear spin ($I = 1/2$ for $^{107}$Ag and $I = 3/2$ for $^{197}$Au). In Table III we present the calculated magnetic resonance parameters for the silver and gold cationic clusters, and it can be seen that the isotropic molecular *g* tensors are in good agreement with the experimental values[9,10] reported for $Ag_3^{2+}$. A more quantitative comparison is hampered because core polarization effects are not included in these restricted DSW calculations. However, if the deviation of the experimental *g* tensor from the spin-only value of 2.0023, viz. $\Delta g(\text{exp}) = -0.0293$ is compared with the $\Delta g(\text{calc}) = -0.0022$, which is obtained as the difference between the relativistic (DSW) and the NR limit results

TABLE III. Magnetic resonance parameters[a] for $Ag_3^{2+}$ and $Au_3^{2+}$.

| | DSW | NR | Experiment[b] |
|---|---|---|---|
| $^{107}Ag_3^{2+}$ | | | |
| $g$: | 1.7071 | 1.7093 | 1.9730 |
| $\Delta g$: | −0.0022[c] | | −0.0293 |
| $A_{\text{Fermi}}$: | −229 | −179 | |
| | | | −203 |
| $A_{\text{hf}}$: | −235[d] | −183 | |
| $^{197}Au_3^{2+}$ | | | |
| $g$:$zz$ | 2.7826 | | |
| | | 1.6988 | |
| $xx=yy$ | 2.3073 | | |
| $A_{\text{Fermi}}$: | 9 | 153 | |
| $A_{\text{hf}}$:$zz$ | 21 | | |
| $xx=yy$ | 7 | 154 | |

[a] Hyperfine values in G.
[b] Experiments (Refs. 9 and 10) show no resolved anisotropy.
[c] $\Delta g$ (calc) value by subtracting DSW from NR, see the text.
[d] $A_{\text{hf}}$ as defined in Eq. (4) in the text.

TABLE IV. Excitation energies (in $cm^{-1}$) for cationic clusters.

| Cluster | Assignment | Excitation energy |
|---|---|---|
| $Ag_3^{2+}$ | $6e_1 \rightarrow 6e_2$ | 24 054 |
| | $6e_1 \rightarrow 6e_3$ | 24 339 |
| $Au_3^{+}$ | $6e_1 \rightarrow 6e_2$ | 17 099 |
| | $6e_1 \rightarrow 6e_3$ | 19 438 |
| | $6e_1 \rightarrow 7e_2$ | 43 795 |
| | $6e_1 \rightarrow 7e_3$ | 51 215 |
| $Au_3^{2+}$ | $6e_1 \rightarrow 6e_2$ | 23 228 |
| | $6e_1 \rightarrow 6e_3$ | 25 406 |
| | $6e_1 \rightarrow 7e_2$ | 55 570 |
| | $6e_1 \rightarrow 7e_3$ | 60 813 |
| $Au_4^{+}$ | $7q \rightarrow 4e_3$ | 14 847 |
| | $4e_3 \rightarrow 9q$ | 33 632 |
| | $4e_3 \rightarrow 5e_2$ | 36 536 |
| $Au_4^{2+}$ | $7q \rightarrow 4e_3$ | 17 744 |
| | $7q \rightarrow 8q$ | 21 696 |
| | $7q \rightarrow 9q$ | 54 361 |
| | $7q \rightarrow 5e_2$ | 57 587 |

(this approach has been shown to give good agreement with the experiment in actinides complexes[38]), a very good agreement is obtained. A slight underestimation of the $\Delta g$(calc) is consistent with the neglect of spin-polarization effects. Nevertheless, the results are close enough to the experimental values and indicate that the DSW method is useful for understanding Zeeman interactions in metallic clusters. Furthermore, the calculated Ag hyperfine tensors, as can be seen in Table III, are also isotropic. We report an approximate Fermi term ($A_{\text{Fermi}}$) and the total $A$ values. An approximate "Fermi" term[21] (which reduces to the conventional Fermi term in the NR limit) can be determined from the DSW calculations as the diagonal contribution from the $s_{1/2}$ orbitals. The DSW calculated value of $A_{\text{Fermi}}$ ($-229$ G) is in fairly close agreement with the observed value ($-203$ G). Furthermore, both the DSW and NR calculated values for the total hyperfine tensors, show small anisotropies (6 and 4 G) which have not been resolved experimentally.[9,10] These small anisotropies arise probably due to the small contributions of the $5p$ ($5p_{3/2}$) and $4d$ ($4d_{3/2}$,$4d_{5/2}$) orbitals to the HOMO $6e_1$. Besides, the small $\Delta g$ values indicates a very small orbital contribution ($\sim 2$ G) to the total hyperfine tensor. However, the major differences between the DSW and the NR results for hyperfine tensors arise from the Fermi term, the larger DSW values indicate a greater $5s_{1/2}$ spin density at the Ag nuclei, as expected due to relativity. In Table III we also predict the magnetic resonance parameters for $Au_3^{2+}$, and several interesting comparisons with $Ag_3^{2+}$ can be made. It should be remarked that the nuclear $g_N$ factors for silver and gold are of opposite sign, which will be reflected in all the metal hyperfine tensors. The calculated NR values of the hyperfine tensors for both $Ag_3^{2+}$ and $Au_3^{2+}$ are nearly the same and this is consistent with the similar nonrelativistic HOMO ($3a_1'$) which is a bonding $s$–$p$ hybrid in both the clusters. However the calculated DSW values indicate a very different paramagnetic behavior, viz. the hyperfine tensors for $Ag_3^{2+}$ are virtually isotropic while for $Au_3^{2+}$ these are mostly anisotropic and furthermore, the $g$ tensors differ considerably. This different paramagnetic behavior of $Au_3^{2+}$ can be understood because the HOMO $6e_1$ is an antibonding MO which consists of combinations of almost pure $5d_{5/2}$ orbitals (see Fig. 6) and therefore, the anisotropic contributions to the $g$ and hyperfine tensors are expected to be very significant. This is borne out by the present DSW calculations shown in Table III. Since the NR ($3a_1'$) and the DSW ($6e_1$) HOMO's of $Au_3^{2+}$ are totally different in character, it is not possible to make a direct comparison between the DSW and the NR values for $Au_3^{2+}$ as is possible for $Ag_3^{2+}$. It can be concluded that the relativistic effects on Zeeman and hyperfine interactions are very significant in the $Au_3^{2+}$ cluster.

## V. TRANSITION STATE CALCULATIONS

The predicted excitation energies for the electronic transitions from the ground state to the unoccupied orbitals (mainly $s$–$p$ hybrids) were calculated by the Slater transition state method[27] and are collected in Table IV. The HOMO–LUMO transition for both the $Ag_3^{2+}$ and $Au_3^{2+}$ clusters absorbs in the violet region of the spectrum. For the gold clusters, it can be seen that, as charge is depleted from the HOMO's, there is a shift from the yellow to the blue region for the lowest electronic transition; whereas for the highest excitation energies ($d_{5/2} \rightarrow p_{1/2} + p_{3/2}$), there are shifts to the lowest part of the UV region. The other excitation energies for $Au_4^{+}$ are from the antibonding (mostly $d_{5/2}$) HOMO and the $6s$–$6p$ unoccupied hybrid orbitals. As cluster size increases (from $Au_3^{2+}$ to $Au_4^{2+}$), one observes

TABLE V. Predicted first ionization potential for clusters.

| Cluster | HOMO | First I.P. (eV) |
|---|---|---|
| $Ag_3^{2+}$ | $(6e_1)^1$ | 19.40 |
| $Au_3^{+}$ | $(6e_1)^2$ | 14.91 |
| $Au_3^{2+}$ | $(6e_1)^1$ | 21.92 |
| $Au_4^{+}$ | $(4e_3)^1$ | 13.23 |
| $Au_4^{2+}$ | $(7q)^4$ | 20.60 |

that the HOMO–LUMO transition occurs at higher wavelengths, and a similar trend is seen for the other electronic transitions. The calculated first ionization potentials (I.P.) are shown in Table V and it can be seen that, as charge is depleted, the molecular systems experience a relaxation of $\sim 7.0$ eV and, furthermore, as the cluster size increases there is a slight decrease in the first I.P.

## VI. CONCLUSIONS

The results presented here represent applications of the Dirac scattered-wave method to study the nature of bonding and prediction of the optical spectra, magnetic properties, and first ionization potentials for the trinuclear and the tetranuclear cationic silver and gold clusters. It is pointed out that nonrelativistic calculations of the gold clusters *in particular* give an unrealistic description of the bonding since it has been shown here that there is very significant *sd* hybridization in bonding which is primarily a relativistic effect. Furthermore, the electronic transitions that are common to $Au_3^{q+}$ and $Au_4^{q+}$ are predicted to be blue shifted with increasing positive charge on the clusters, and the first ionization potential decreases as the cluster size increases. The geometries of these gold clusters are not yet known; however, the trends of the type mentioned here are expected to be important in the analysis of the optical absorption and ESR spectra of these gold clusters.

In conclusion, the DSW method can be very useful for an understanding of bonding trends, photoelectron, optical absorption, and ESR spectra for metallic clusters containing atoms too large or too heavy for high quality *ab initio* relativistic computations.

## ACKNOWLEDGMENTS

We are grateful to Professor David Case for helpful discussions and to A. Ramos for his assistance with the contour maps. This work was supported by the Natural Sciences and Engineering Research Council of Canada by a Grant (No. A3598).

[1]Faraday Symp. Chem. Soc. **14**, 1–350 (1980).
[2]Ber. Bunsenges. Phys. Chem. **88**, 220–273 (1984).
[3]Proceedings from a Symposium on Small Particles and Metallic Clusters, Surf. Sci. **156**, (1985), Parts I and II.
[4]M. D. Morse, M. E. Gensic, J. R. Health, and R. E. Smalley, J. Chem. Phys. **83**, 2293 (1985).
[5]M. D. Morse, J. B. Hopkins, P. R. Langridge-Smith, and R. E. Smalley, J. Chem. Phys. **79**, 5316 (1983).
[6]K. Kernisant, G. A. Thompson, and D. M. Lindsay, J. Chem. Phys. **82**, 4739 (1985); J. A. Howard, K. F. Preston, and B. Mile, J. Am. Chem. Soc. **103**, 6226 (1981).
[7]H. Basch, J. Am. Chem. Soc. **103**, 4657 (1981).
[8]J. Flad, G. Igel-Mann, H. Preuss, and H. Stoll, Chem. Phys. **90**, 257 (1984).
[9]C. E. Forbes and M. C. R. Symons, Mol. Phys. **27**, 467 (1974).
[10]D. R. Brown, T. J. V. Findlay, and M. C. R. Symons, J. Chem. Soc. Dalton Trans. I **72**, 1792 (1976).
[11]P. Sudraud, C. Colliex, and J. van de Walle, J. Phys. (Paris) Lett. **40**, L207 (1979).
[12]A. R. Waugh, J. Phys. D **13**, L203 (1980).
[13]Th. Jentsch, W. Drachsel, and J. H. Block, Chem. Phys. Lett. **93**, 144 (1982); W. Draschel, Th. Jentsch, K. A. Gingerich, and J. H. Block, Surf. Sci. **156**, 173 (1985).
[14]S. J. Rose, I. P. Grant, and N. C. Pyper, J. Phys. B **11**, 1171 (1978).
[15]*Relativistic Effects in Atoms, Molecules and Solids*, edited by G. L. Malli (Plenum, New York, 1983).
[16]N. C. Pyper and P. Marketos, Mol. Phys. **42**, 1073 (1981).
[17]D. A. Case, Annu. Rev. Phys. Chem. **33**, 151 (1982).
[18]C. Y. Yang, in Ref. 15, p. 335.
[19]C. Y. Yang and D. A. Case, in *Local Density Approximations in Quantum Chemistry*, edited by J. Dahl and J. P. Avery (Plenum, New York, 1984), p. 643.
[20]D. A. Case and C. Y. Yang, J. Chem. Phys. **72**, 344 (1980).
[21]R. Arratia-Perez and D. A. Case, J. Chem. Phys. **79**, 4939 (1983).
[22]C. Y. Yang, R. Arratia-Perez, and J. P. Lopez, Chem. Phys. Lett. **107**, 112 (1984); R. Arratia-Perez and D. A. Case, Inorg. Chem. **23**, 3271 (1984).
[23]D. A. Case and J. P. Lopez, J. Chem. Phys. **80**, 3270 (1984).
[24]J. P. Lopez and D. A. Case, J. Chem. Phys. **81**, 4554 (1984).
[25]R. Arratia-Perez and C. Y. Yang, J. Chem. Phys. **83**, 4005 (1985).
[26]M. E. Rose, *Relativistic Electron Theory* (Wiley, New York, 1961).
[27]J. C. Slater, *Quantum Theory of Molecules and Solids* (McGraw-Hill, New York, 1974), Vol. IV.
[28]J. G. Norman, Jr., Mol. Phys. **31**, 1191 (1976).
[29]K. Schwarz, Phys. Rev. B **5**, 2466 (1972); K. Schwarz, Theor. Chim. Acta **34**, 225 (1974).
[30]G. A. Ozin, H. Huber, D. F. McIntosh, S. A. Mitchell, L. Noodleman, and J. G. Norman, Jr., J. Am. Chem. Soc. **101**, 3504 (1979).
[31]A. D. McLean, J. Chem. Phys. **79**, 3392 (1983).
[32]G. Apai, S. T. Lee, and M. G. Mason, Solid State Commun. **37**, 213 (1981).
[33]S. Rabii and C. Y. Yang, Chem. Phys. Lett. **105**, 480 (1984).
[34]H. Stoll, P. Fuentealba, M. Dolg, J. Flag, L. von Szentpaly, and H. Preuss, J. Chem. Phys. **79**, 5532 (1983).
[35]D. A. Case and M. Karplus, Chem. Phys. Lett. **39**, 33 (1976).
[36]Y. S. Lee, W. C. Ermler, K. S. Pitzer, and A. D. McLean, J. Chem. Phys. **70**, 288 (1979).
[37]C. E. Moore, *Atomic Energy Levels*, Natl. Bur. Stand. No. 474 (U.S. GPO, Washington, D.C., 1952).
[38]D. A. Case, J. Chem. Phys. **83**, 5792 (1985).